Dalton Transactions

Alkaline Earth Metal-Assisted Dinitrogen Activation at Nickel

Journal:	*Dalton Transactions*
Manuscript ID	DT-ART-11-2023-003984.R1
Article Type:	Paper
Date Submitted by the Author:	03-Feb-2024
Complete List of Authors:	Knoell, Theresa; Towson University, Chemistry Polanco, Jocelyn; Towson University, Chemistry MacMillan, Samantha; Cornell University, Chemistry and Chemical Biology Bertke, Jeffery; Georgetown University, Department of Chemistry Foroutan-Nejad, Cina; Polish Academy of Sciences Lancaster, Kyle; Cornell University, Chemistry and Chemical Biology Bakhoda, Abolghasem; Towson University, Department of Chemistry

ARTICLE

Alkaline Earth Metal-Assisted Dinitrogen Activation at Nickel

Theresa Knoell[a],† Jocelyn Polanco[a],† Samantha N. MacMillan[b], Jeffery A. Bertke[c], Cina Foroutan-Nejad[d]*, Kyle M. Lancaster[b]*, and Abolghasem 'Gus' Bakhoda[a]*

Received 00th January 20xx,
Accepted 00th January 20xx

DOI: 10.1039/x0xx00000x

Rare examples of trinuclear [Ni–N_2–M–N_2–Ni] core (M = Ca, Mg) with linear bridged dinitrogen ligands are reported in this work. The reduction of [^{i}Pr$_2$NN]Ni(μ–Br)$_2$Li(thf)$_2$ (**1**) (^{i}Pr$_2$NN = 2,4-bis-(2,6-diisopropylphenylimido)pentyl) with elemental Mg or Ca in THF under an atmosphere of dinitrogen yields the complex {^{i}Pr$_2$NNNi(μ-N_2)}$_2$M (thf)$_4$ (M = Mg, complex **2** and M = Ca, complex **3**). The bridging end-on (μ–N_2)$_2$M(thf)$_4$ moiety connects the two [^{i}Pr$_2$NNNi]$^-$ nickelate fragments. A combination of X-ray crystallography, solution and solid-state spectroscopy have been applied to characterize complexes **2** and **3**, and DFT studies have been used to help explain the bonding and electronic structure in these unique Ni–N_2–Mg and Ni–N_2–Ca complexes.

Introduction

Industrially, the "fixation" of nitrogen to produce ammonia (N_2 + 3 H_2 ⇄ 2 NH_3) through the Haber-Bosch (H-B) process enables sustenance of the world's population.[1–3] H-B is an enormously energy intensive process and accounts for 1.8% of global CO_2 emissions and ca 3% of global energy consumption.[4] This has encouraged a great interest in developing more sustainable ammonia production alternatives. Consequently, coordination, activation, and full dissociation of the N≡N bond of the dinitrogen molecule have become some of the most studied topics in the areas of inorganic and organometallic chemistry.[5–8]

So far, multiple systems based on early to middle transition metals such as Ti[9–12], Zr[13–15], V[16–18], Cr[19–22], Mo[23–26], along with other late transition metals like Fe[27–38], Co[28,39,40], Ru[41,42], and Os[41] have been studied for N_2 to NH_3 transformation under relatively mild conditions. Among these metals, Fe, Mo and W are perhaps the most azophilic metals of the transition series.[43] On the other hand, Ni dinitrogen complexes are rare and therefore, have not been extensively studied in dinitrogen activation and splitting processes.[44] To date, 24 nickel dinitrogen complexes have been isolated and studied crystallographically, most of which are phosphine-supported Ni(0) complexes (Cambridge Structural Database, 2023.2 CSD Software).

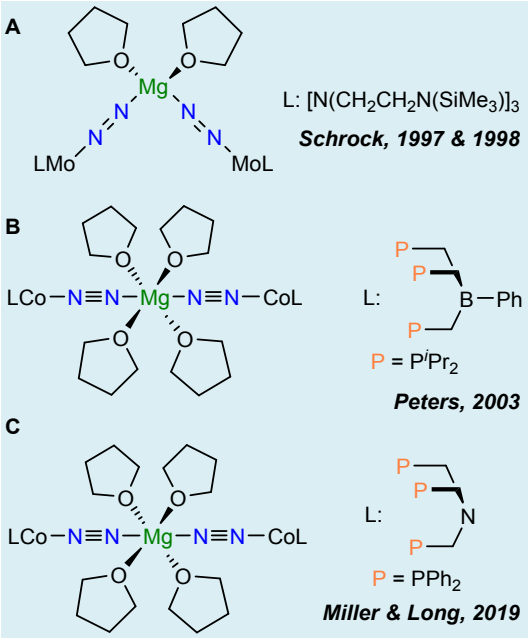

Fig. 1. Previous examples of structurally characterized multinuclear dinitrogen complexes with M–N_2–Mg moiety.

The majority of N_2 to NH_3 transformations require the use of strong reductants such as alkali metals (KC_8, KNap, Na amalgam, Na sand etc). Other reducing agents such as $CoCp_2$, $CoCp^*_2$ $CrCp^*_2$, and

[a] Department of Chemistry Towson University 8000 York Road Towson, MD 21252.
[b] Department of Chemistry and Chemical Biology, Cornell University, Ithaca, NY, USA.
[c] Georgetown University, Department of Chemistry, Washington, DC 20057, USA.
[d] Institute of Organic Chemistry, Polish Academy of Sciences, Kasprzaka 44/52, 01-224 Warsaw, Poland.
† Authors contributed equally to this work.
Electronic Supplementary Information (ESI) available: Additional spectral data and details associated with X-ray diffraction. For ESI and crystallographic data in CIF or other electronic format see DOI: 10.1039/x0xx00000x
§ A. B. would like to dedicate this paper to the memory of Davood Amiri (1972-2022).

Sm^{2+} have also found use in the nitrogen fixation reactions.[45] On the other hand, alkaline earth metals such as Mg have been far less studied as the reductant in ammonia formation from dinitrogen and only a few studies have been reported. [28,31,46–49]

Schrock and co-workers observed a trimetallic Mo–Mg–Mo system (Figure 1A) supported by triamidoamine ligands for the activation of dinitrogen to diazenide (N_2^{2-}).[50,51] Peters et al. used an anionic tris(phosphine)borate ligand to isolate a trimetallic system consisting of two Co(0) centers with a linear LCo–N_2–Mg–N_2–CoL core (Figure 1B).[28] Later, Miller and Long reported the synthesis of a Co(-I) congener N_2 complex supported by triphos ligand (Figure 1C).[52] In 2013, Holland and co-workers reported the activation of dinitrogen over a multimetallic system with a linear $L^{tBu}Co–N_2–Mg–N_2–CoL^{tBu}$ and $L^{tBu}Fe–N_2–Mg–N_2–Fe$ L^{tBu} (L^{tBu} = a bulky β-diketiminate ligand).[31] They reacted $[L^{tBu}]Co^{II}–Cl$ with Rieke magnesium (Mg*) in THF and were able to isolate $\{L^{tBu}Co(\mu\text{-}N_2)\}_2Mg(thf)_4\}$ in only 6% yield. Although Holland and co-workers were able to successfully confirm the trinuclear $\{L^{tBu}Co(\mu\text{-}N_2)\}_2Mg(thf)_4\}$ structure via elemental analysis and IR spectroscopy, their attempts to obtain high quality X-ray crystallographic data were unsuccessful. In the same report, they also reported an attempt to isolate the analogous Fe complex $\{L^{tBu}Fe(\mu\text{-}N_2)\}_2Mg(thf)_4\}$, however this molecule was shown to be metastable and structural analysis was not possible. The only structurally characterized complexes with the M–N_2–AE–N_2–M scaffold (M = transition metal and AE = alkaline earth metal) are limited to those reported by Peters[28] and Miller and Long[52] where M = Co and AE = Mg.

We sought to study the reduction of a β-diketimanato Ni(II) complex $[^iPr_2NN]Ni(\mu–Br)_2Li(thf)_2$[53] with alkaline earth metals Mg and Ca to investigate the reduction and activation of the N–N bond in dinitrogen at Ni center. Herein, we report the synthesis and characterization of the first examples of Ni dinitrogen complexes bridged with alkaline metals Mg and Ca. These complexes possess a linear Ni–N_2–AE–N_2–Ni (AE = Mg and Ca) core and their solution and solid-state structures were elucidated.

Results and discussion

Synthesis and spectroscopy of $\{^iPr_2NNNi(\mu\text{-}N_2)\}_2Mg(thf)_4$ and $\{^iPr_2NNNi(\mu\text{-}N_2)\}_2Ca(thf)_4$

The reduction of the $[^iPr_2NN]Ni(\mu–Br)_2Li(thf)_2$ (**1**) starting material[53] with magnesium turnings in anhydrous THF under an atmosphere of dinitrogen inside a glovebox resulted in the formation of $\{^iPr_2NNNi(\mu\text{-}N_2)\}_2Mg(thf)_4$ (**2**) that is a new trimetallic dinitrogen complex with bridging N_2 ligands. During this reduction the solution changed color from dark violet-blue of **1** to deep red within 30-45 min. The complex **2** was crystallized from *n*-pentane to furnish dark red crystals of $\{^iPr_2NNNi(\mu\text{-}N_2)\}_2Mg(thf)_4$ (**2**) in 56% (Figure 2). Full characterization of **2** including the crystal structure determination, is provided in the Supporting Information. Freshly prepared $\{^iPr_2NNNi(\mu\text{-}N_2)\}_2Mg(thf)_4$ (**2**) in THF exhibited a ν_{NN} band in IR spectrum at 1923 cm^{-1}, while in the solid state the N–N bond stretching frequency was observed at 1920 cm^{-1}. In addition, we investigated the UV-Vis absorption spectra of **2** in both THF and *n*-pentane. In both cases, a band at 521 nm was observed (Supporting Information). It is noteworthy that complex **2** is EPR silent both in solution (*n*-pentane) and in the solid state, perhaps due to zero-field splitting as a result of the spin–spin coupling. Dissolving complex **2** in solvents such as benzene or toluene resulted in an immediate gas effervescence (presumably displacement of N_2 ligand by the solvent) and results in the formation of $[(^iPr_2NNNi)_2(\mu\text{-}$

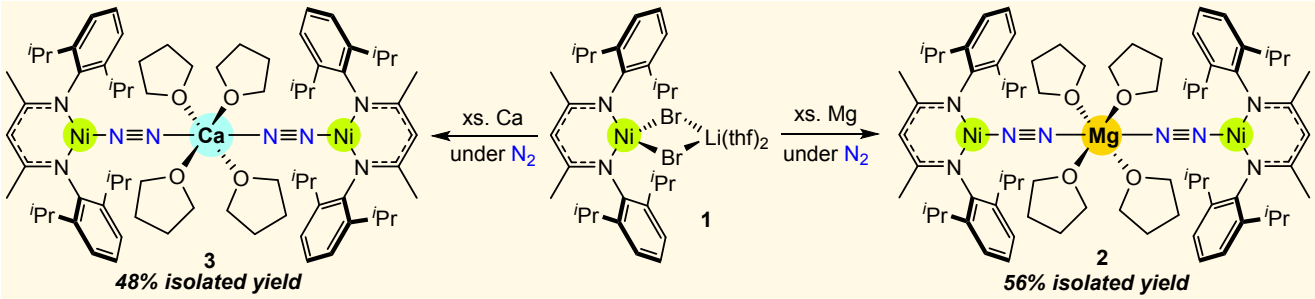

Fig. 2. Synthesis of Dinitrogen Complexes $\{^iPr_2NNNi(\mu\text{-}N_2)\}_2Mg(thf)_4$ (**2**) and $\{^iPr_2NNNi(\mu\text{-}N_2)\}_2Ca(thf)_4$ (**3**).

η^3:η^3-C_6H_6)] or [(^{i}Pr$_2$NNNi)$_2$(μ-η^3:η^3-C_6H_5Me)] (**4**), a previously reported complex by Stephan and co-workers.[53] Upon standing in solution at room temperature, a color change from red to pale green is observed for complex **2** with the precipitation of a black powdered solid, presumably Ni black. However, **2** is stable enough in solution to be studied by ^{1}H NMR spectroscopy. In cyclohexane-d^{12} **2** shows a fully interpretable ^{1}H and ^{13}C NMR spectra (Supporting Information) and no paramagnetism was observed in solution (Evan's method[54]).

Interestingly, we were able to repeat the reduction of [^{i}Pr$_2$NN]Ni(μ–Br)$_2$Li(thf)$_2$ (**1**) with calcium turnings to obtain {^{i}Pr$_2$NNNi(μ-N$_2$)}$_2$Ca(thf)$_4$ (**3**) in 48% yield as dark red crystals (Figure 2). Full characterization of **3** including the crystal structure, is also provided in the Supporting Information. Similar to complex **2**, freshly prepared **3** in THF shows a band at 1921 cm^{-1} in its IR spectrum that can be attributed to the N–N bond stretch, while in the crystalline state this band was observed at 1916 cm^{-1}. The UV-vis absorption spectra of **3** in both THF and *n*-pentane revealed two bands at 498 and 658 nm (Supporting Information). While complex **3** is less stable in solution than **2**, we were able to obtain ^{1}H and ^{13}C NMR spectra in cyclohexane-d^{12} (Supporting Information). Like **2**, complex **3** is also EPR silent and is diamagnetic in solution (Evan's method). It is noteworthy that **3** is the first dinitrogen complex of the transition metals capped by Ca^{2+} ion as a Lewis-acid.

Comparing the IR spectra of [LM–N$_2$–Mg–N$_2$–ML] from Holland's work[31] and what is observed for complexes **2** and **3** of this report, (where L is β-diketiminate ligand and M = Fe, Co, and Ni), it can be concluded that the degrees of dinitrogen activation decreases moving from Fe to Ni (Table 1). For the Fe congener, the frequency of the N–N band was observed at 1808 cm^{-1}, showing a more activated N_2 ligand, followed by ν_{NN} of 1878 and 1923 cm^{-1} for the Co and Ni complexes. The weaker extension of dinitrogen reduction can be attributed to the weaker degrees of backbonding interaction of the late transition metals such as Ni. With respect to the role of Lewis acid in activation of the N_2 ligand, no significant changes are observed. This observation is reminiscent of what was observed for similar systems investigated by Limberg et al.[55,56] Limberg et al. prepared a series of Ni–N_2 complexes with general formula of M_2[LNi(μ-η^1:η^1-N$_2$)NiL] (M = Na, K, Na/K) and showed that the alkali metal cations coordinated to the N_2 units do not significantly contribute to the extent of N_2 activation (See Table 1). It is noteworthy that the extent of dinitrogen reduction was higher when alkali metals were used (Limberg's system) than those with alkaline earth metals (current report).

Table 1. Metrical parameters and N–N stretching frequencies for dinitrogen complexes of the Fe, Co and Ni supported by β-diketiminate ligands.

Complex*	ν_{NN} [cm^{-1}]	N–N [Å]	Reference
Mg[L$_2$Fe(N$_2$)$_2$]	1808	N/A	30
Mg[L$_2$Co(N$_2$)$_2$]	1878	N/A	30
Mg[L$_2$Ni(N$_2$)$_2$] (**2**)	1923	1.115(9)	*This work*
Na$_2$[L$_2$Ni(N$_2$)$_2$]	1685	1.192(3)	52
K$_2$[L$_2$Ni(N$_2$)$_2$]	1696	1.185(8)	53
NaK[L$_2$Ni(N$_2$)$_2$]	1689	1.195(4)	52

X-ray crystal structures of {^{i}Pr$_2$NNNi(μ-N$_2$)}$_2$Mg(thf)$_4$ (2) and {^{i}Pr$_2$NNNi(μ-N$_2$)}$_2$Ca(thf)$_4$ (3)

X-ray crystal structures of **2** and **3** are presented in Figure 3. Single crystals of **2** were grown in *n*-pentane at -35 °C inside of a

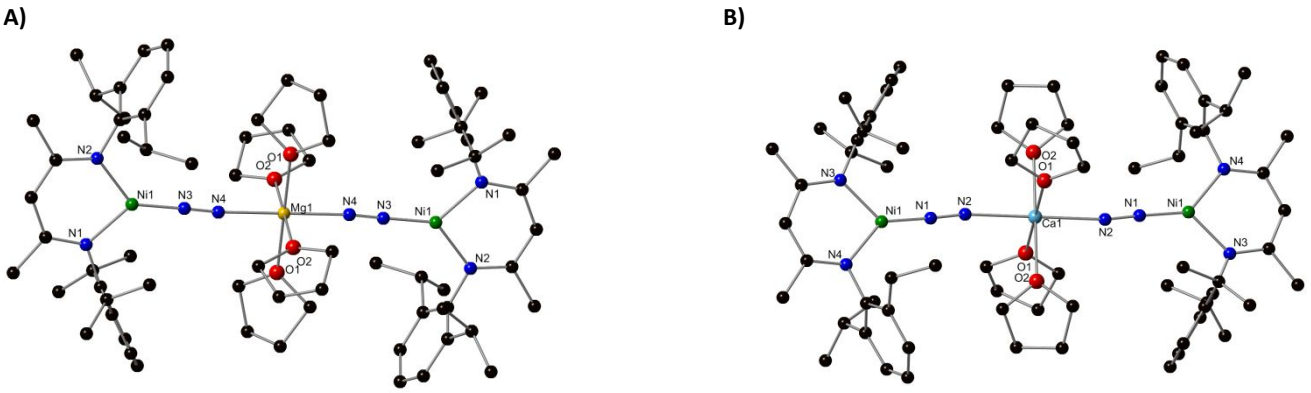

Fig. 3. A) POV-ray depiction of the complexes **2** (A) and **3** (B). The hydrogen atoms and *n*-pentane solvent molecules are omitted for clarity.

glovebox freezer. X-ray analysis of **2** shows a dumbbell like structure via an assembly of a linear LNi–N≡N–Mg–N≡N–NiL (L = 2,4-bis-(2,6-diisopropylphenylimido)-2,4-pentyl) core, with a stabilizing central Mg atom bridging between two Ni–N_2 complexes (Figure 3A). The crystal structure of {^{i}Pr$_2$NNNi(μ-N$_2$)}$_2$Mg(thf)$_4$ is in fact a co-crystal of **2** and 5% of a side product, namely [^{i}Pr$_2$NN]NiBr. This complex is only evident at the Br site which overlaps with the bridging N_2 moiety of **2**. The [^{i}Pr$_2$NN]Ni moieties of each species occupy the same sites in the crystalline lattice. Refinement of this data as pure **2** results in a residual electron density peak of nearly one electron in extremely close proximity to N4 as well as a short N–N distance < 1.00 Å. Inclusion of this 5% co-crystalline model may seem insignificant, but for these reasons we believe it to be the most complete and accurate model for the data. The Ni–N≡N–Mg–N≡N–Ni core shows an almost linear Co–N–N bonds N–N–Mg bonds (178.4(6) and 173.5(7), respectively). These values are typical for the Lewis acid coordinated dinitrogen ligands.[57] The Ni–N_{N2} was observed at 1.688(5) Å and the Mg–N_{N2} bond lengths were determined to be 2.082(6) and 2.083(6). The X-ray analysis of **2** also reveals that the N–N bond length is 1.115(9) Å that is elongated relative to the free N_2 (N–N = 1.0975 Å[7]), indicating a significant N_2 activation. This is also confirmed by the low ν_{NN} band in **2** in its IR spectrum (1923 cm^{-1}).

Crystals of complex **3** were grown similarly from a chilled solution of **3** in *n*-pentane. Like complex **2**, a linear LNi–N≡N–Ca–N≡N–NiL moiety was corroborated by X-ray diffraction analysis of the single crystals of complex **3** (Figure 3B). The N_2 ligand in **3** exhibits an N–N bond length of 1.163(4) Å that is slightly longer than that of

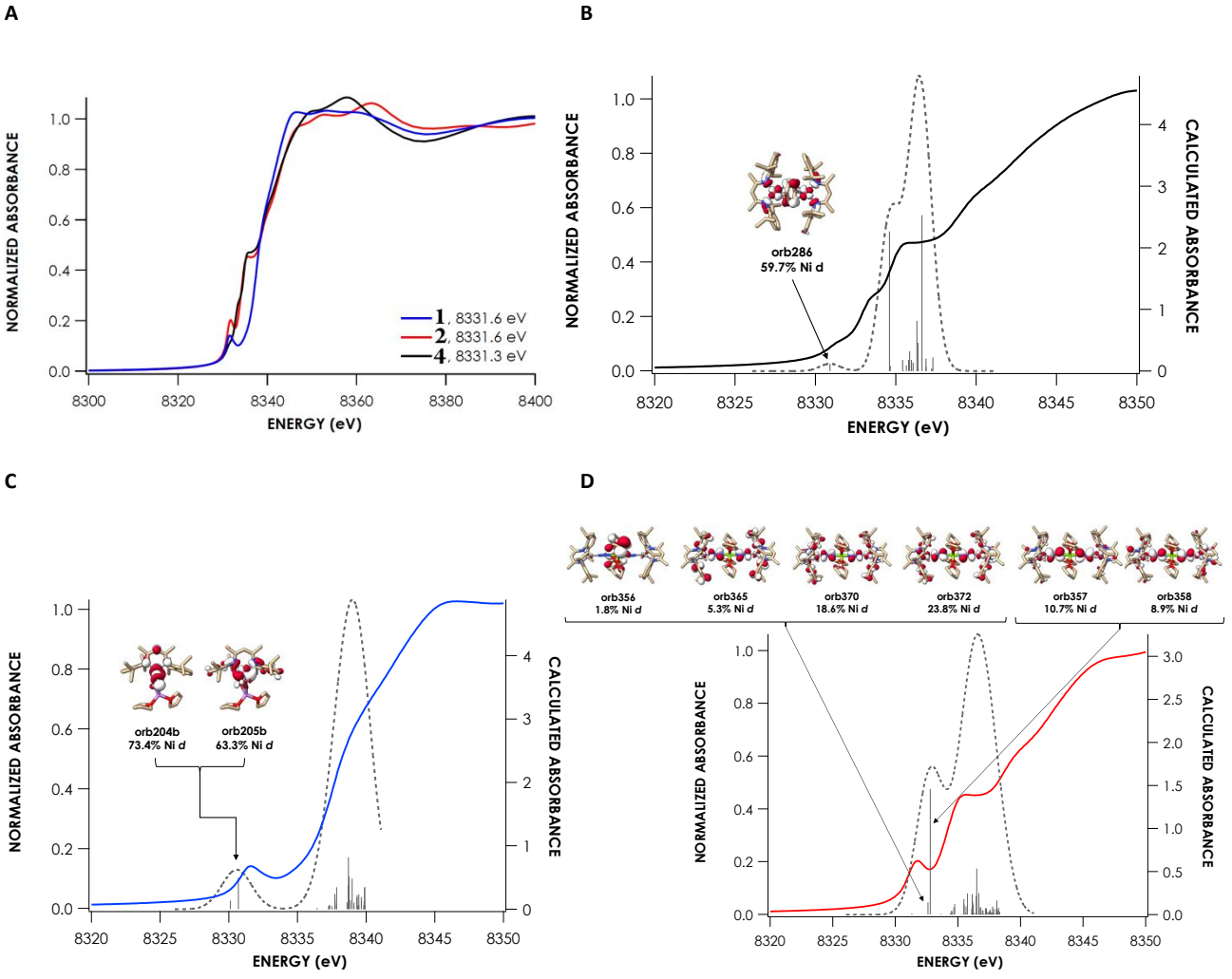

Fig. 4. A**)** Ni K-edge XAS of compounds **1**,**2** and **4**. B) Experimental (black) and TDDFT-calculated (gray, dashed) Ni K-edge XAS of **4**. Dominant acceptor molecular orbitals contributing to individual transitions (sticks) are plotted at an isovalue of 0.03 au. C) Experimental (black) and TDDFT-calculated (gray, dashed) Ni K-edge XAS of **1**. Dominant acceptor molecular orbitals contributing to individual transitions (sticks) are plotted at an isovalue of 0.03 au. D) Experimental (black) and TDDFT-calculated (gray, dashed) Ni K-edge XAS of **2**. Dominant acceptor molecular orbitals contributing to individual transitions (sticks) are plotted at an isovalue of 0.03 au.

complex **2** (1.115(9) Å). This value is consistent with similar levels of N_2 activation in compound **3**, which showed a band at 1921 cm^{-1} in the IR spectrum for ν_{NN}. In the solid state, **3** shows an almost linear Ni–N–N bond while the N–N–Ca bond is slightly bent [178.0(3) and 169.9(3), respectively]. The Ni–N_{N2} bond length was 1.906(2) Å and the Ca–N_{N2} bond length was 2.299(3) Å in the X-ray crystal structure of **3**. Both **2** and **3** contained the Lewis acid Mg (in **2**) or Ca (in **3**) in an octahedral environment and were ligated by two *trans* N_2 and four thf ligands.

Electronic Structure of $\{^{i}Pr_2NNNi(\mu\text{-}N_2)\}_2Mg(thf)_4$ (2) and $\{^{i}Pr_2NNNi(\mu\text{-}N_2)\}_2Ca(thf)_4$ (3)

Density functional theory (DFT) computations at PBE0[58,59]/def2-SVP[60] level suggests that a closed-shell diradical solution, obtained from the broken-symmetry DFT, provides the lowest energy for both **2** and **3** compared to the closed-shell solution. The open-shell singlet electronic structure is lower in energy than the closed-shell electronic structure by 4.4 and 4.5 kcal mol^{-1} for complexes **2** and **3**, respectively, at our computational level after correction for zero-point energies. To perform BS-DFT we broke the complexes into three fragments: a neutral singlet $M(N_2)_2(thf)_4$ fragment (M = Mg or Ca), and two neutral, doublet LNi(I) fragments with opposite spins. To further investigate the electronic structure, we utilized XAS analysis. For more information see Supporting Information.

We were profoundly interested in the electronic structures of complexes **2** and **3**. Due to its higher thermal stability, we chose to analyze complex **2** by Ni K-edge XAS with interpretation facilitated by comparison to Ni(I) and Ni(II) standards as well as using time-dependent density functional theory calculations (TDDFT). The X-ray crystal structure of the title compound was revised to include occupational disorder of N_2 vs bromide (See Supporting Information). Additional analysis was carried out using Mg 1s X-ray photoelectron spectroscopy (XPS).

Normalized Ni K-edge XAS for compounds $[LNi^{II}(\mu\text{–}Br)_2Li(thf)_2]$(**1**), $\{LNNNi(\mu\text{-}N_2)\}_2Mg(thf)_4$ (**2**), and $[LNNNi^{I}_2(arene)]$ (**4**), where L = [^{i}PrNN] are shown in Figure 4A. All species display pre-edge features. These occur at 8331.3 eV for complex **1** and 8331.6 eV for complexes **2** and **4**. The spectra of **2** and **4** display two additional rising edge features between 8333 eV and 8337 eV. Complex **4** is a formally Ni(I) species; complex **1** is a formally Ni(II) complex. The similarity in pre-edge peak energies for **2** and **4** would conventionally suggest that **2** be assigned as bearing Ni(II) centers. However, we and others have shown that trends in K-edge XAS energies alone should not be considered diagnostic of physical oxidation states, especially when there are differences in coordination environment.[61–63] A particularly notable complication arises due to the presence of unoccupied molecular orbitals of predominantly ligand character that bear admixture from transition metal valence *d* or *p* orbitals. Given that plausible formulations for $\{LNNNi(\mu\text{-}N_2)\}_2Mg(thf)_4$ span the gamut of Ni oxidation states from 0 to +2, we sought first to establish the oxidation state of the bridging Mg center and to inform ourselves with electronic structure calculations. Mg 1s XPS data (Supporting Information) were obtained to address this. The value obtained for the Mg 1s binding energy in compound **2** is 1304.17 eV. This value is consistent with divalent magnesium. Reported values for Mg(0) (as Mg metal) range from 1303 eV to 1303.6 eV[64],while Mg(II) as MgO ranges from 1304.2–1305.0; $MgCl_2•6H_2O$, and MgF_2 appear at 1304.8 and 1304.95 eV, respectively.[65,66]

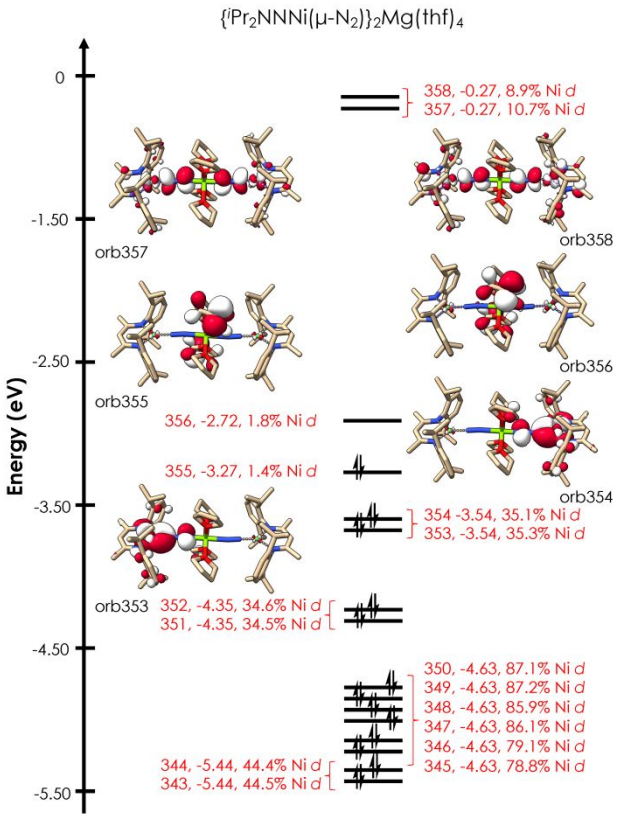

Fig. 5. Frontier molecular orbital diagram for **2**. Orbitals are plotted at an isovalue of 0.03 au.

Table 2. The delocalization indices, DI, bond lengths in Å, localization indices, LI, atomic and fragment charges, q(A), and atomic and fragment spin densities $|\rho_s(A)|$ of studied complexes obtained from broken-symmetry DFT computations by breaking the complexes into three fragments, two LNi(I) and one $M(N_2)_2$. Regular and bold numbers represent values computed via QTAIM and fuzzy atomic partitioning, respectively.

Complexes	DI(Ni, N)	BL(Ni, N)	DI(N, N)	BL(N,N)	DI(N, M)	LI(Ni)	q(Ni)	$q(N_2)$	$\|\rho_s(Ni)\|$	$\|\rho_s(N_2)\|$
Complex 2	1.19 **1.58**	1.695	2.32 **2.33**	1.162	0.11 **0.58**	25.63 **26.51**	0.728	-0.861	0.67	0.66
Complex 3	1.18 **1.57**	1.695	2.33 **2.35**	1.163	0.20 **0.52**	25.62 **26.49**	0.735	-0.847	0.67	0.66

DFT calculations were carried out using the B3LYP hybrid density functional along with all-electron basis sets on all atoms. Single point solutions were then used as the starting point for time-dependent DFT (TDDFT) calculations of the Ni K-edge XAS. To account for systematic errors in calculations of the Ni 1s potential, a scalar shift of 6.07 eV was applied to each spectrum. This value was obtained by taking the average difference between calculated and experimental peak positions, as has been described previously.[67] All calculated spectra show good agreement with experimental data (Figures 4B-D), providing confidence in the veracity of the calculated electronic structures and prompting further scrutiny of the electronic structure of **2**. A frontier molecular orbital diagram for **2** is shown in Figure 5.

A key finding is that the pre-edge features in the K-edge XAS of **2** feature contributions from promotions to numerous unoccupied orbitals bearing some Ni 3d character. Our prior studies of Ni 3d vacancies using Ni $L_{2,3}$-edge XAS demonstrated strong agreement between calculated and experimental values.[63] In the present case, summing this Ni character reveals total Ni 3d vacancy of 1.4 electrons. Divided over the two Ni centers, this is a 3d vacancy of 0.7 per Ni, indicating an oxidation state slightly more reduced than Ni(I). This accords with a previous proposal by Wolczanski that Ni centers in coordination complexes bear charges within ca. 0.5 e of +1.3.[68] Assuming monoanionic β-diketiminate ligand, and given the Mg assignment from XPS as Mg(II), this supports partial reduction of the bridging N_2 fragments, consistent with the diminished N–N stretching frequencies relative to the free N_2.

Consequently, the assembled results support a best formulation of the compound in question as bearing a Mg(II) bridge, and N_2 molecules activated via π-back bonding to an extent that the Ni oxidation state is best formulated as intermediate between Ni(0) and Ni(I). Ni(I) however, is most consistent with our DFT calculations that suggest the complexes have open-shell singlet electronic structures.

Bonding Analysis

We studied the nature of metal–nitrogen bonding within the context of the quantum theory of atoms in molecules, QTAIM[69] and fuzzy atomic space using Becke's method of multicenter numerical integration.[70,71] The QTAIM delocalization index (DI) just like its fuzzy atom counterpart measures the number of shared electrons between a pair of atoms. The DI can be interpreted as the covalent bond order in the case of homonuclear bonds. However, it deviates from the formal covalent bond order as the electronegativity difference between the interacting atoms increases. In a fully ionic bond, the DI approaches zero.[72] In the present case both QTAIM and fuzzy delocalization index values agree well with each other. However, fuzzy DI is larger for the interaction between the dinitrogen and Mg or Ca. Localization indices obtained from the fuzzy space partitioning are more consistent with the picture of a Ni(I) oxidation state than those of the topological QTIAM partitioning as discussed elsewhere.[73,74]

The delocalization index for the N–N bond in all complexes is reduced to 2.3 in line with nearly 0.8 e additional charge on N_2 upon coordination to the Ni center in the presence of the alkaline earth metals, Mg and Ca (Table 2). In complexes **2** and **3**, each {LNNNi(μ-N_2)} fragment receives an electron from the Mg^{2+} (in **2**) or Ca^{2+} (in **3**) at the center of the molecule, which pairs with the free electron on the Ni(I) centers. This additional bond influences other local electronic indicators of bonding in the {LNNNi(μ-N_2)}$_2$Mg(thf)$_4$ (M = Mg or Ca) complexes. The dinitrogen fragments in both molecules **2** and **3** sustain a spin density comparable with that of Ni centers with the opposite spin (Figure 6). It is worth noting that for a closed-shell system spin density is an arbitrary parameter that

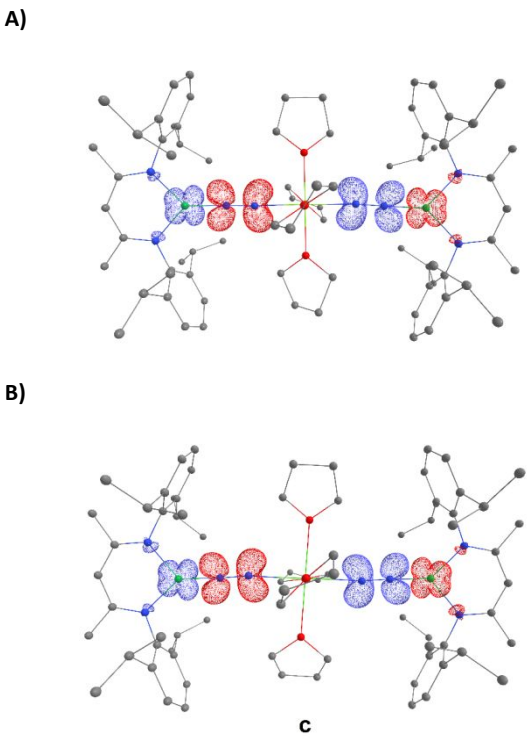

Fig. 6. Spin density maps of (A) {$^{i}Pr_2NNNi(\mu\text{-}N_2)\}_2Mg(thf)_4$ (**2**) and, (B) {$^{i}Pr_2NNNi(\mu\text{-}N_2)\}_2Ca(thf)_4$ (**3**) with an isodensity surface of 0.005 au (1 au = 1 electron) obtained from broken-symmetry DFT computations for closed-shell singlet species. The complexes are fragmented to two LNi^{I} and $M(N_2)_2$ fragments for BS-DFT computations. Hydrogen atoms are omitted for clarity.

merely approximates local electron density if we dismiss the indistinguishability principle of electrons. Although, arbitrary, generating spin densities from broken-symmetry DFT computations can help to draw a chemical picture of bonding. Here, the spin density plots show the coupling between the two electrons that are transferred from the alkaline earth metals in the center of the complexes and Ni(I) centers.

Experimental

General considerations

Experiments were performed under an atmosphere of dinitrogen in a glove box. All organic solvents were dried over activated 4 Å molecular sieves and were stored under nitrogen atmosphere inside a glove box. Cyclohexane-d_{12} was passed through a Pasteur pipette containing powdered activated molecular sieves and then degassed via three freeze–pump–thaw cycles and stored over molecular 4 Å sieves. All other reagents were purchased from the commercial sources and used as received. Nuclear magnetic resonance (NMR) experiments were performed on a JOEL 400 SS spectrometer (400 MHz) spectrometer. All chemical shifts (δ) for ^{1}H and ^{13}C are relative to solvent's residual proton (1.38 ppm in ^{1}H and 26.43 ppm in ^{13}C NMR) and are reported in parts per million (ppm).

Synthesis of {$^{i}Pr_2NNNi(\mu\text{-}N_2)\}_2Mg(thf)_4$ (2)

Inside a dry box filled with dry dinitrogen, [$^{i}Pr_2NN]Ni(\mu\text{-}Br)_2Li(thf)_2$][53] (551 mg, 0.700 mmol) was dissolved in anhydrous THF (15 mL) to give a dark violet-blue solution. To this solution was added Mg turnings (97.9 mg, 3.5 mmol, 5 equiv.) and the mixture was stirred at room temperature. A dark red color was observed after 30-45 min. The stirring was continued for 5 h and then the dark red mixture was filtered through a pad of celite. The cherry red solution was dried under reduced pressure to yield the crude product. As much of the crude product as possible was dissolved in anhydrous *n*-pentane (~ 15 mL), and the mixture was filtered through syringe filter to remove a small amount of insoluble brownish material. The dark red solution was stored at –35 °C freezer inside the dry box to give dark red crystals that were suitable for X-ray crystallography (274 mg, 0.197 mmol, 56 %). $C_{79}H_{126}MgN_8Ni_2O_4$ (1390.85): calcd. C, 68.09; H, 9.11; N, 8.04; found C 67.93, H 9.19, N 8.09. The EA was performed on a sample that was crystallized multiple times from *n*-pentane to remove the [$^{i}Pr_2NN]NiBr$ impurity. FT-IR (THF Solution, cm^{-1}): 3055, 2960, 2925, 2866, 1923, 1622, 1551, 1460, 1436, 1395, 1382, 1362, 1319, 1259, 1254, 1192, 1175, 1100, 1051, 1044, 934, 912, 888, 795, 758. ^{1}H NMR (400 MHz, Cyclohexane-d_{12}) δ 7.04–6.90 (m, 9H), 6.76 (t, 4H), 4.22 (s, 2H), 3.63–3.57 (m, 24 H), 1.70–1.65 (m, 16 H), 1.44 (d, 12 H), 1.19 (d, 24H). ^{13}C NMR (101 MHz, Cyclohexane-d_{12}) δ 156.14, 151.95, 140.02, 121.87, 121.66, 92.60, 66.87, 27.64, 26.91, 26.15, 24.00, 23.92, 22.63, 21.84.

Synthesis of {$^{i}Pr_2NNNi(\mu\text{-}N_2)\}_2Ca(thf)_4$ (3)

Inside a dry box filled with dry dinitrogen, [$^{i}Pr_2NN]Ni(\mu\text{-}Br)_2Li(thf)_2$] (551 mg, 0.700 mmol) was dissolved in anhydrous THF (15 mL) to give a dark violet-blue solution. To this solution was added Ca turnings (140 mg, 3.5 mmol, 5 equiv.) and the mixture was stirred at room temperature. A dark red color was observed after 3–4 h. The stirring was continued for 8 h before the dark red mixture was filtered through a pad of celite. The red solution was then dried under dynamic vacuum to yield

the crude product. As much of the residue as possible was dissolved in anhydrous *n*-pentane (~ 15 mL), and the mixture was filtered through syringe filter to remove a small amount of insoluble brownish material. The dark red solution was stored at –35 °C freezer inside the dry box to furnish dark red crystals of **3** that were suitable for X-ray crystallography (237 mg, 0.168 mmol, 48 %). Elemental analysis: $C_{79}H_{126}CaN_8Ni_2O_4$ (1406.82): calcd. C, 67.32; H, 9.01; N, 7.95; found C 67.44, H 9.08, N 8.03. FT-IR (THF Solution, cm^{-1}): 3050, 2954, 2863, 1921, 1621, 1530, 1515, 1439, 1414, 1409, 1360, 1320, 1254, 1249, 1175, 1099, 1055, 1041, 923, 897, 886, 762, 758, 714. ^{1}H NMR (400 MHz, Cyclohexane-d_{12}) δ 6.98 – 6.92 (m, 8H), 6.82 – 6.87 (m, 2H), 6.79 – 6.75 (m, 2H), 4.59 (s, 1H), 4.17 (s, 1H), 3.64 (sept, 4H), 3.16 (sept, 4H), 3.04 (br, 16H), 1.52 (br, 16H), 1.52 (d, 7H), 1.20–1.16 (m, 24H), 1.01 (d, 11H). ^{13}C NMR (101 MHz, Cyclohexane-d_{12}) δ 162.64, 148.93, 140.41, 140.18, 122.41, 122.17, 121.93, 92.20, 67.43, 27.50, 26.16, 24.12, 23.75, 22.74, 22.02.

Conclusions

We have shown that alkaline earth metals such as magnesium and calcium can be used as reductants for Ni(II) complexes supported by a β-diketiminate ligand, and the reduction leads to the formation of heterotrimetallic dinitrogen complexes with a linear LNi–N≡N–M–N≡N–NiL core (L = β-diketiminate ligand, M = Mg and Ca) in complexes **2** and **3**. We also reported the first example of a transition metal-dinitrogen complex with an end-on Ca-capped dinitrogen fragment (complex **3**). The IR data of **2** and **3** are in agreement with those of the few reported congener examples in the literature. The results of this work highlight the ability of alkaline earth metals such as Mg and Ca to reduce dinitrogen at low-valent nickel centers. The analysis of electronic structure of **2** via K-edge XAS, XPS, and DFT calculations suggests that alkaline earth metals reduce both the bridging N_2 ligand fragments as well as the Ni centers with an oxidation state close to Ni(I). We expect that the results of this work will be useful in the design of future late-metal systems for the activation of dinitrogen using alkaline earth metals.

Data availability

All the other specific experimental procedures, spectral and crystallographic details of the compounds are given in the ESI.† Crystallographic data for compounds **2** and **3** has been deposited as CCDC 2283060 and 2283061 respectively.†

Author Contributions

A. B. conceived and designed the experiments. T. K., J. P. and A. B. carried out the experiments. S. N. MacMillan and K. M. L. performed the XAS experiments and interpreted the data. J. A. B. performed the X-ray crystallographic work. C. F. -N. conceived and performed the bonding analysis.

‡T.K. and J.P. contributed equally to this work.

Conflicts of interest

There are no conflicts to declare.

Acknowledgements

C.F.-N. thanks to National Science Centre, Poland 2020/39/B/ST4/02022 for funding his work and thanks Polish high-performance computing infrastructure PLGrid (HPC Centers: ACK Cyfronet AGH) for providing computer facilities and support within computational grant no. PLG/2023/016855. KML gratefully acknowledges NIGMS (R35-GM124908). Use of the Stanford Synchrotron Radiation Lightsource, SLAC National Accelerator Laboratory, is supported by the U.S. Department of Energy, Office of Science, Office of Basic Energy Sciences under Contract No. DE-AC02-76SF00515. The SSRL Structural Molecular Biology Program is supported by the DOE Office of Biological and Environmental Research, and by the National Institutes of Health, National Institute of General Medical Sciences (P30GM133894). A.B. gratefully acknowledges the financial support from Towson University through research grants from the Fisher College of Science and Mathematics (FCSM). This work was also supported by instrumentation provided through the National Science Foundation under Grant No. 0923051.

Notes and references

1 V. S. Marakatti and E. M. Gaigneaux, *ChemCatChem*, 2020, **12**, 5838–5857.
2 H. Hosono and M. Kitano, *Chem. Rev.*, 2021, **121**, 3121–3185.
3 T.-N. Ye, S.-W. Park, Y. Lu, J. Li, M. Sasase, M. Kitano, T. Tada and H. Hosono, *Nature*, 2020, **583**, 391–395.

4 J. G. Chen, R. M. Crooks, L. C. Seefeldt, K. L. Bren, R. M. Bullock, M. Y. Darensbourg, P. L. Holland, B. Hoffman, M. J. Janik, A. K. Jones, M. G. Kanatzidis, P. King, K. M. Lancaster, S. V. Lymar, P. Pfromm, W. F. Schneider and R. R. Schrock, *Science*, 2018, **360**, eaar6611.
5 Y. Tanabe and Y. Nishibayashi, *Coord. Chem. Rev.*, 2022, **472**, 214783.
6 M. J. Chalkley, M. W. Drover and J. C. Peters, *Chem. Rev.*, 2020, **120**, 5582–5636.
7 B. A. MacKay and M. D. Fryzuk, *Chem. Rev.*, 2004, **104**, 385–402.
8 D. Bora, F. R. Gayen and B. Saha, *RSC Adv.*, 2022, **12**, 33567–33583.
9 D. Y. Bae, G. Lee and E. Lee, *Inorg. Chem.*, 2021, **60**, 12813–12822.
10 L. R. Doyle, A. J. Wooles, L. C. Jenkins, F. Tuna, E. J. L. McInnes and S. T. Liddle, *Angew. Chem. Int. Ed.*, 2018, **57**, 6314–6318.
11 T. Shima, S. Hu, G. Luo, X. Kang, Y. Luo and Z. Hou, *Science*, 2013, **340**, 1549–1552.
12 L. R. Doyle, A. J. Wooles and S. T. Liddle, *Angew. Chem. Int. Ed.*, 2019, **58**, 6674–6677.
13 J. A. Pool, E. Lobkovsky and P. J. Chirik, *Nature*, 2004, **427**, 527–530.
14 D. Pun, E. Lobkovsky and P. J. Chirik, *J. Am. Chem. Soc.*, 2008, **130**, 6047–6054.
15 Y. Sekiguchi, F. Meng, H. Tanaka, A. Eizawa, K. Arashiba, K. Nakajima, K. Yoshizawa and Y. Nishibayashi, *Dalton Trans.*, 2018, **47**, 11322–11326.
16 Y. Kokubo, C. Yamamoto, K. Tsuzuki, T. Nagai, A. Katayama, T. Ohta, T. Ogura, Y. Wasada-Tsutsui, Y. Kajita, S. Kugimiya and H. Masuda, *Inorg. Chem.*, 2018, **57**, 11884–11894.
17 Y. Sekiguchi, K. Arashiba, H. Tanaka, A. Eizawa, K. Nakajima, K. Yoshizawa and Y. Nishibayashi, *Angew. Chem. Int. Ed.*, 2018, **57**, 9064–9068.
18 Y. Kokubo, Y. Wasada-Tsutsui, S. Yomura, S. Yanagisawa, M. Kubo, S. Kugimiya, Y. Kajita, T. Ozawa and H. Masuda, *Eur. J. Inorg. Chem.*, 2020, **2020**, 1456–1464.
19 I. Vidyaratne, J. Scott, S. Gambarotta and P. H. M. Budzelaar, *Inorg. Chem.*, 2007, **46**, 7040–7049.
20 A. J. Kendall and M. T. Mock, *Eur. J. Inorg. Chem.*, 2020, **2020**, 1358–1375.
21 Y. Ashida, A. Egi, K. Arashiba, H. Tanaka, T. Mitsumoto, S. Kuriyama, K. Yoshizawa and Y. Nishibayashi, *Chem. A Eur. J.*, 2022, **25**, e202200557 .
22 Z.-B. Yin, B. Wu, G.-X. Wang, J. Wei and Z. Xi, *J. Am. Chem. Soc.*, 2023, **145**, 7065–7070.
23 D. V. Yandulov and R. R. Schrock, *Science*, 2003, **301**, 76–78.
24 K. C. MacLeod and P. L. Holland, *Nature Chem*, 2013, **5**, 559–565.
25 R. R. Schrock, *Acc. Chem. Res.*, 2005, **38**, 955–962.
26 Y. Tanabe and Y. Nishibayashi, *Coord. Chem. Rev.*, 2019, **389**, 73–93.
27 J. S. Anderson, J. Rittle and J. C. Peters, *Nature*, 2013, **501**, 84–87.
28 T. A. Betley and J. C. Peters, *J. Am. Chem. Soc.*, 2003, **125**, 10782–10783.
29 T. M. Buscagan, P. H. Oyala and J. C. Peters, *Angew. Chem. Int. Ed.*, 2017, **56**, 6921–6926.
30 M. J. Dorantes, J. T. Moore, E. Bill, B. Mienert and C. C. Lu, *Chem. Commun.*, 2020, **56**, 11030–11033.
31 T. R. Dugan, K. C. MacLeod, W. W. Brennessel and P. L. Holland, *Eur. J. Inorg. Chem.*, 2013, **2013**, 3891–3897.
32 J. Higuchi, S. Kuriyama, A. Eizawa, K. Arashiba, K. Nakajima and Y. Nishibayashi, *Dalton Trans.*, 2018, **47**, 1117–1121.
33 S. Kuriyama, K. Arashiba, K. Nakajima, Y. Matsuo, H. Tanaka, K. Ishii, K. Yoshizawa and Y. Nishibayashi, *Nat. Commun.*, 2016, **7**, 12181.
34 D. J. Schild and J. C. Peters, *ACS Catal.*, 2019, **9**, 4286–4295.
35 J. Fajardo and J. C. Peters, *Inorg. Chem.*, 2021, **60**, 1220–1227.
36 M. Reiners, D. Baabe, K. Münster, M.-K. Zaretzke, M. Freytag, P. G. Jones, Y. Coppel, S. Bontemps, I. D. Rosal, L. Maron and M. D. Walter, *Nat. Chem.*, 2020, **12**, 740–746.
37 N. Hazari, *Chem. Soc. Rev.*, 2010, **39**, 4044.
38 J. L. Crossland and D. R. Tyler, *Coord. Chem. Rev.*, 2010, **254**, 1883–1894.
39 T. J. Del Castillo, N. B. Thompson, D. L. M. Suess, G. Ung and J. C. Peters, *Inorg. Chem.*, 2015, **54**, 9256–9262.
40 S. Kuriyama, K. Arashiba, H. Tanaka, Y. Matsuo, K. Nakajima, K. Yoshizawa and Y. Nishibayashi, *Angew. Chem. Int. Ed.*, 2016, **55**, 14291–14295.
41 J. Fajardo and J. C. Peters, *J. Am. Chem. Soc.*, 2017, **139**, 16105–16108.
42 D. Allen and C. V. Senoff, .
43 Y. Nishibayashi, Ed., *Nitrogen Fixation*, Springer International Publishing, Cham, 2017, vol. **60**.
44 K. L. Gullett, J. W. Nugent, W. T. Darrow, D. C. Najera, N. A. Bender, E. L. Bruske, C. A. Leahy, T. J. Miller, S. R. Muhammad and A. R. Fout, in *Comprehensive Coordination Chemistry III*, Elsevier, 2021, pp. 188–228.
45 Q. Wang, J. Guo and P. Chen, *Chem*, 2021, **7**, 3203–3220.
46 K. Yuvaraj, A. Paparo, A. J. R. Matthews and C. Jones, *Eur. J. Inor. Chem.*, 2021, **2021**, 4998–5003.
47 B. Rösch, T. X. Gentner, J. Langer, C. Färber, J. Eyselein, L. Zhao, C. Ding, G. Frenking and S. Harder, *Science*, 2021, **371**, 1125–1128.
48 R. Mondal, K. Yuvaraj, T. Rajeshkumar, L. Maron and C. Jones, *Chem. Commun.*, 2022, **58**, 12665–12668.
49 R. Mondal, M. J. Evans, T. Rajeshkumar, L. Maron and C. Jones, *Angew. Chem. Int. Ed.*, 2023, e202308347.
50 M. B. O'Donoghue, N. C. Zanetti, W. M. Davis and R. R. Schrock, *J. Am. Chem. Soc.*, 1997, **119**, 2753–2754.
51 M. B. O'Donoghue, W. M. Davis and R. R. Schrock, *Inorg. Chem.*, 1998, **37**, 5149–5158.
52 S. L. Apps, P. W. Miller and N. J. Long, *Chem. Commun.*, 2019, **55**, 6579–6582.
53 G. Bai, P. Wei and D. W. Stephan, *Organometallics*, 2005, **24**, 5901–5908.
54 D. F. Evans, *J. Chem. Soc.*, 1959, 2003.
55 B. Horn, S. Pfirrmann, C. Limberg, C. Herwig, B. Braun, S. Mebs and R. Metzinger, *Z. anorg. allg. Chem.*, 2011, **637**, 1169–1174.
56 S. Pfirrmann, C. Limberg, C. Herwig, R. Stößer and B. Ziemer, *Angew. Chem. Int. Ed.*, 2009, **48**, 3357–3361.
57 A. Simonneau and M. Etienne, *Chem. Eur. J.*, 2018, **24**, 12458–12463.
58 M. Ernzerhof and G. E. Scuseria, *J. Chem. Phys.*, 1999, **110**, 5029–5036.
59 C. Adamo and V. Barone, *J. Chem. Phys.*, 1999, **110**, 6158–6170.
60 F. Weigend, *Phys. Chem. Chem. Phys.*, 2006, **8**, 1057.
61 N. C. Tomson, K. D. Williams, X. Dai, S. Sproules, S. DeBeer, T. H. Warren and K. Wieghardt, *Chem. Sci.*, 2015, **6**, 2474–2487.
62 I. M. DiMucci, J. T. Lukens, S. Chatterjee, K. M. Carsch, C. J. Titus, S. J. Lee, D. Nordlund, T. A. Betley, S. N. MacMillan and K. M. Lancaster, *J. Am. Chem. Soc.*, 2019, **141**, 18508–18520.

63 I. M. DiMucci, C. J. Titus, D. Nordlund, J. R. Bour, E. Chong, D. P. Grigas, C.-H. Hu, M. D. Kosobokov, C. D. Martin, L. M. Mirica, N. Nebra, D. A. Vicic, L. L. Yorks, S. Yruegas, S. N. MacMillan, J. Shearer and K. M. Lancaster, *Chem. Sci.*, 2023, **14**, 6915–6929.
64 N. C. Haider, J. Alonso and W. E. Swartz, *Z. Naturforsch. A*, 1975, **30**, 1485–1490.
65 H. Seyama and M. Soma, *J. Chem. Soc., Faraday Trans. 1*, 1984, **80**, 237.
66 C. D. Wagner, *J. Electron Spectrosc. Relat. Phenom.*, 1980, **18**, 345–349.
67 S. DeBeer George, T. Petrenko and F. Neese, *J. Phys. Chem. A*, 2008, **112**, 12936–12943.
68 P. T. Wolczanski, *Organometallics*, 2017, **36**, 622–631.
69
70 I. Mayer and P. Salvador, *Chem. Phys. Lett.*, 2004, **383**, 368–375.
71 A. D. Becke, *J. Chem. Phys.*, 1988, **88**, 2547–2553.
72 S. Sowlati-Hashjin, V. Šadek, S. Sadjadi, M. Karttunen, A. Martín-Pendás and C. Foroutan-Nejad, *Nat. Commun.*, 2022, **13**, 2069.
73 C. S. Day, C. D. Do, C. Odena, J. Benet-Buchholz, L. Xu, C. Foroutan-Nejad, K. H. Hopmann and R. Martin, *J. Am. Chem. Soc.*, 2022, **144**, 13109–13117.
74 J. Mehara, A. Koovakattil Surendran, T. van Wieringen, D. Setia, C. Foroutan-Nejad, M. Straka, L. Rulíšek and J. Roithová, *Chem. Eur. J.*, 2022, **28**, e202201794.